Escape of Mars Photoionized Electrons from Carbon Dioxide and Atomic Oxygen in 2004

R. A. Frahm,[a] J. R. Sharber,[a] J. D. Winningham,[a] S. J. Jeffers,[a] C. A. Gonzalez,[a] J. Mukherjee,[a] M. Muller,[a] J. R. Scherrer,[a]
R. Link,[b] M. W. Liemohn,[c] J. U. Kozyra,[c] A. J. Coates,[d] D. R. Linder,[d] S. Barabash,[e] R. Lundin,[e] A. Fedorov [f]

[a] Southwest Research Institute, PO Drawer 28510, 6220 Culebra Road, San Antonio, TX, USA, [b] Radiation Safety Institute of Canada, 1120 Finch Ave. W., Suite 607, Toronto On, M3J-3H7, Canada
[c] Space Pyhsics Research Laboratory, University of Michigan, Ann Arbor, MI 48109-2143, USA, [d] Mullard Space Science Laboratory, University College London, Surrey RH5 6NT, UK
[e] Swedish Institute of Space Physics, Box 812, SE-981 28, Kiruna, Sweden, [f] Centre d'Etude Spatiale des Rayonnements, BP-4346, F-31028, Toulouse, France

Abstract

Photoelectron peaks in the atmosphere caused by the ionization of carbon dioxide and atomic oxygen by solar 30.4 nm photons have been observed by the Electron Spectrometer (ELS), a component of the Mars Express (MEx) Analyzer of Space Plasmas and Energetic Atoms (ASPERA-3) Experiment. Ionization occurs mostly at the Mars exobase with the majority of the photoionized electron flux trapped in the remanent magnetic field and a portion of that flux escaping the planet down its tail. Observations of photoelectron spectra in the ionosphere and tail indicate that the spacecraft is variably charged. Absolute flux in the tail can be examined by adjusting the electron spectra for the spacecraft charge. A background photoelectron flux of the adjusted spectra is estimated in the region of the electron spectrum that shows photoelectron peaks and this background is removed, yielding a flux of about 5.74×10^6 electrons/(cm^2 s sr) escaping Mars. The number of ELS sectors which show the photoelectron peak signature is typically between 1 and 3, which is on average an plasma acceptance cone of about 22.5° or 0.478 sr. This gives a flux for the sample spectrum of about 2.74×10^7 electrons/(cm^2 s). The sample spectrum from the tail has a distinct shape similar to those in the ionosphere. In 2004, the frequency of occurrence statistics show about a 9% occurrence rate for only those types of spectra resembling similar shaped ionization peaks. The sample of distinct photoelectron flux is estimated to be the same as the average 2004 photoelectron flux, which yields an average rate of escape from Mars of 2.47×10^7 electrons/(cm^2 s) during 2004. By estimating the outflow area of 1.16×10^{19} cm^2 at 1.5 R_{Mars}, the electron escape rate of 2.85×10^{27} electrons/s is determined. This means that about 8.99×10^{30} electrons or 15 Mmole of electrons escaped Mars in 2004 due to the ionization of carbon dioxide and atomic oxygen by the He 30.4 nm line. Electron escape rates should reflect the escape rate of ions in order to maintain charge neutrality. Due to the caveats of the analysis, these derived escape rates should be considered lower limits on the total electron escape rate from Mars.

1. Introduction

As part of the solar wind-Mars interaction, some of the atmosphere of Mars is stripped away from the planet. This escaping plasma was found to be lost at differing rates using ion measurements from various spacecraft missions. Using ion measurements from the Phobos-2 mission obtained near solar maximum, Lundin *et al.* [1989, 1990] estimated the total escape of about 3×10^{25} s^{-1} while Verigin *et al.* [1991] determined the loss of ions from the plasma sheet to be about 5×10^{25} s^{-1}. From the Mars Express (MEx) spacecraft at solar minimum, Dubinin *et al.* [2006] found a total escape rate of between 6×10^{25} s^{-1} and 6×10^{26} s^{-1} while Carlsson *et al.* [2006], using scaled escape rates from the Phobos-2 spacecraft [Lundin *et al.*, 1989], estimated the CO_2^+ loss rate to be 4.0×10^{26} s^{-1}. Barabash *et al.* [2007] refined these numbers to determine an O^+ loss rate of 1.6×10^{25} s^{-1}, an O_2^+ loss rate of 1.5×10^{25} s^{-1}, and a CO_2^+ loss rate of 8×10^{25} s^{-1}. Mars atmospheric erosion rates determined so far have been preformed using ion measurements. Mars atmospheric erosion rates determined using electron measurements are difficult because the bulk flow velocities are low and measurements are often influenced by the presence of spacecraft. Electron escape rates should reflect the escape rate of ions in order to maintain charge neutrality.

Since December 25, 2003, the MEx spacecraft has been orbiting Mars. MEx measurements of the Martian particle environment have been performed by the Analyzer of Space Plasmas and Energetic Atoms (ASPERA-3) Experiment [Barabash *et al.*, 2004; 2006], which measures electrons with the Electron Spectrometer (ELS), ions with the Ion Mass Analyzer (IMA), and neutral particles with the Neutral Particle Detector (NPD) and Neutral Particle Imager (NPI). Since arriving at Mars, ELS has measured peaks in the photoelectron spectrum [Lundin *et al.*, 2004]. These photoelectron peaks are attributed to both carbon dioxide and atomic oxygen, and are theoretically located in energy between 21 eV and 24 eV, and 27 eV [Mantas and Hanson, 1979; Fox and Dalgarno, 1979]. The relevant photoelectron peaks in the energy spectrum are mainly due to ionization by solar 30.4 nm photons. More specifically for carbon dioxide the following ionizations are described by Padial *et al.* [1981] and the ejected photoelectron is computed for a solar 30.4 nm photon:

$$CO_2 + h\nu \longrightarrow CO_2^+ + e^- \begin{cases} X^2\Pi_g \text{ ionization potential } 13.8 \text{ eV} \longrightarrow 27.0 \text{ eV electron} \\ A^2\Pi_u \text{ ionization potential } 17.7 \text{ eV} \longrightarrow 23.1 \text{ eV electron} \\ B^2\Sigma_u^+ \text{ ionization potential } 18.1 \text{ eV} \longrightarrow 22.7 \text{ eV electron} \\ C^2\Sigma_g^+ \text{ ionization potential } 19.4 \text{ eV} \longrightarrow 21.4 \text{ eV electron} \end{cases} \quad (1$$

Ta0806_ALL

For atomic oxygen, the ionization states are described by Mantas and Hanson [1979] and the ejected photoelectron is also computed for a solar 30.4 nm photon:

$$O + h\nu \longrightarrow O^+ + e^- \begin{cases} ^4S \text{ ionization potential } 13.62 \text{ eV} \longrightarrow 27.16 \text{ eV electron} \\ ^2D \text{ ionization potential } 17.10 \text{ eV} \longrightarrow 23.68 \text{ eV electron} \\ ^2P \text{ ionization potential } 18.50 \text{ eV} \longrightarrow 22.28 \text{ eV electron} \end{cases} \quad (2$$

Ta0806_ALL

The ELS observation of photoelectron peaks in the energy spectrum are mainly due to ionization of carbon dioxide near the Martian exobase [Mantas and Hanson, 1979]. Near the Martian exobase, the concentration of carbon dioxide is about 50 times greater than atomic oxygen. After ionization of the carbon dioxide or atomic oxygen, the charged components are subject to the local magnetic field and are transported accordingly. The ASPERA-3 ELS has observed photoelectron peaks in the Martian induced magnetosphere while orbiting the planet at various altitudes [Frahm *et al*, 2006a,b; Liemohn *et al.*, 2006a,b].

2. Data

Photoelectron peaks are observed on almost every transit of the spacecraft through the dayside ionosphere. Figure 1 shows an orbit of the MEx spacecraft on 19 June 2007 in cylindrical Mars-centered Solar Orbital (MSO) coordinates (the X-axis points toward the Sun, The Z-axis is perpendicular to the planet's velocity vector in the northern ecliptic plane, and the Y-axis completes the right handed system). On this figure, the Sun is at the left. The average shapes of the bow shock and magnetopause are determined by Vignes *et al.* [2000] are drawn in blue. The trajectory of MEx is marked in red with tick marks every 10 minutes and time labels every hour. The pericenter of MEx is marked with a green circle and orbit numbers are computed at apocenter crossings, which is marked with two green circles on the MEx trajectory. Vertical black lines break the MEx trajectory, with orbit 4439 being shown prior to 1906 UT and orbit 4440 being shown after 1906 UT (the orbit number counter definition occurs at the location of the apocenter markings). The general locations where photoelectron peaks are observed in the electron spectrum are shown as shaded regions along the spacecraft orbit.

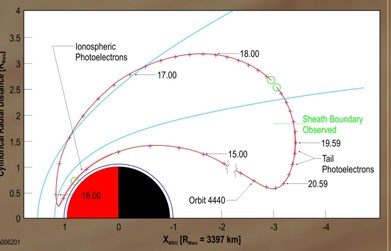

Figure 1. The orbit of MEx is shown on 19 June 2007. The MEx trajectory is shown in MSO coordinates as a red curve, ticked at 10 min intervals and labeled every UT hour. Included are highlighted regions where measurements of photoelectron peaks in the ionosphere and tail are generally observed on this spacecraft orbit. The bow shock and magnetopause are drawn for reference using Vignes et al. [2000].

In this pass, the ELS data place the location of the magnetopause at a lower radial distance to the X-axis than the average position predicted by Vignes *et al.* [2000]. The location of the magnetopause derived from the ELS data is noted on Figure 1 in green. This pass was chosen because electron spectra showing carbon dioxide and atomic oxygen photoionization peaks are observed both in the dayside ionosphere and far down the tail of Mars.

2.1. Photoelectron Peaks Observed in the Martian Ionosphere

The spacecraft enters the ionosphere from the night side of the planet and measures peaks in the photoelectron spectrum beginning at about 1535 UT (625 km altitude) until it exits into the dayside magnetosheath around 1558 UT (725 km altitude). A more detailed view can be obtained by examining the combined ion and electron spectrogram. Figure 2 shows the ion spectrogram measured by IMA sector 0 (IMA-00) in the top panel and the electron spectrogram measured by ELS sector 4 (ELS-04) in the bottom panel. At this time, IMA is observing low-energy ions in its fast sample rate mode (96 energy measurements from 10 eV to 30 keV in 12 sec); its elevation analyzer is not stepping. This mode allows 2D ion measurements to be determined at a faster repetition rate than when its elevation analyzer is scanning. ELS is also measuring in its fast sample rate mode (31 energy measurements from 9 eV to 150 eV in 1 sec), and the ASPERA-3 scanner is parked. This condition also generates a 2D ELS measurement.

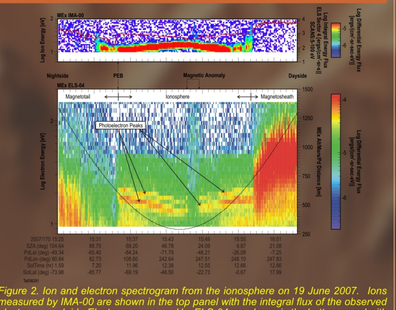

Figure 2. Ion and electron spectrogram from the ionosphere on 19 June 2007. Ions measured by IMA-00 are shown in the top panel with the integral flux of the observed electrons overlaid. Electrons measured by ELS-04 are shown in the bottom panel with the altitude of MEx overlaid. The solar zenith angle (SZA), planetodetic latitude (PdLat), planetodetic longitude (PdLon), solar time (SolTime), and solar latitude (SolLat) of the spacecraft is given along the bottom.

In Figure 2, the photoionization peaks observed in the electron spectrogram from carbon dioxide and atomic oxygen are seen in the ionosphere at the same time that low-energy ions are observed. The peaks in the electron spectrogram are observed to decrease in energy with decreasing altitude, and at the same time the trace in ion flux increases in energy. These patterns indicate that during this pass, the Spacecraft charges negatively, forcing the detected electrons to decelerate and lose energy as they fall to the spacecraft. At the same time, the ions are accelerated as they fall through the potential well created by the spacecraft charge. The amount of spacecraft charging becomes a larger negative value as the spacecraft altitude approaches the pericenter altitude, about 290 km, indicated by a change in the energy location of the peaks from photoionization of carbon dioxide and atomic oxygen.

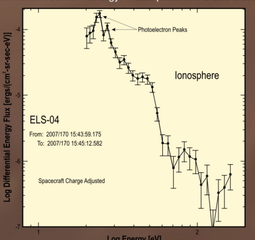

Figure 3. Dayside ionospheric differential energy flux spectrum. The energy flux is adjusted for the estimated -10.8 volt spacecraft charge. Error bars are also shown on this plot and include (1) Poisson statistics, (2) telemetry compression uncertainties, and (3) instrument uncertainties. Instrument uncertainties include uncertainties derived from the (1) physical geometric factor, (2) microchannel plate transparency, (3) protection grid transparency, (4) active anode area ratio, (5) accumulation time, (6) energy resolution, (7) relative microchannel plate efficiency, and (8) Bordoni efficiency [Bordoni, 1971].

2.2. Photoelectron Peaks Observed in the Martian Tail

The orbit of the spacecraft causes it to exit the dayside of the ionosphere, pass through the bow shock, and enter the solar wind before reentering the magnetosheath on the night side in the deep tail (10,000 km altitude). The section of the orbit in the tail encompassing the inner magnetospheric boundary (IMB) is presented in Figure 4. In this figure, the spacecraft data begins in the magnetosheath (1931 UT) at an altitude of about 10,000 km and concludes (2031 UT) in the Martian tail at an altitude of about 8,400 km. The format of Figure 4 is in the same as Figure 2.

The character of the electrons in the magnetosheath shows oscillations in the flux, resembling a series of closely bunched electron beams. Just after the inner magnetosheath boundary is crossed, there is a decrease in the electron flux and then a slight increase between about 1956 UT and 2014 UT (about 9,600 - 9,000 km altitude). The flux increases again between about 2018 UT and 2024 UT (about 8,900 - 8,700 km) before again decreasing in intensity. Between about 2018 UT and 2024 UT, photoelectron peaks are observed in the electron energy spectrum which are termed "distinct" and between about 1956 UT and 2014 UT one peak is observed and termed "degraded".

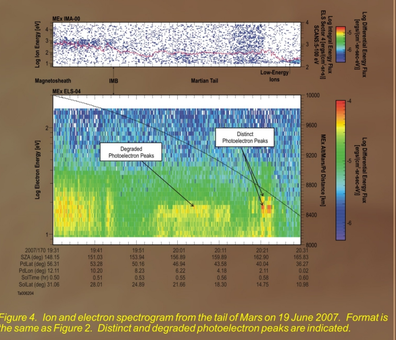

Figure 4. Ion and electron spectrogram from the tail of Mars on 19 June 2007. Format is the same as Figure 2. Distinct and degraded photoelectron peaks are indicated.

2.2.1. Distinct Photoelectron Peaks

Figure 5 shows distinct photoelectron peaks observed in the Martian tail for ELS sector 4. The format is similar to that of Figure 3. In this case, ELS sector 4 is viewing progressively nearly parallel to the inner magnetosheath boundary, toward the Sun, and toward Mars. Presented is the differential energy flux spectrum averaged between 20:22:59 UT through 20:24:08 UT, so again about 50 spectral measurements are averaged. Comparison of this tail spectrum with that measured in the ionosphere shows similarity below 60 eV, which implies that ionospheric plasma is flowing away from the planet. In particular, the photoelectron peaks of carbon dioxide and atomic oxygen are created near the exobase on the day side of the planet where the densities are large enough to generate distinct electron peaks in the energy spectrum, so spectra showing these distinct photoelectron features must come from the dayside.

2.2.2. Degraded Photoelectron Peaks

Some measurements in the Martian tail exhibit electron spectra in which the peaks in energy are not distinct. For these cases, the two peak structure of the carbon dioxide and atomic oxygen photoelectrons is merged into one broad peak, showing energy degradation. This spectrum is shown in Figure 6 for ELS sector 4. The format is similar to that of Figure 3. In this case, ELS sector 4 is viewing nearly in the same direction as when distinct photoelectron peaks are observed. Presented is the differential energy flux spectrum averaged between 20:01:59 UT through 20:03:08 UT, so again about 50 spectral measurements are averaged. Statistics accumulated to date do not include a contribution from spectra showing degraded peaks since they would not have been recognized as a peak structure. Thus, the rates calculated from our statistics will under-represent the actual loss.

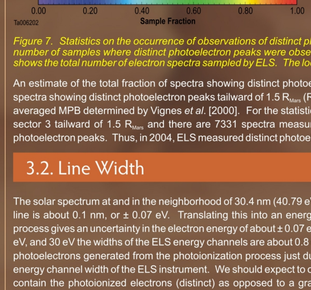

Figure 5. Adjusted tail electron spectra showing distinct photoelectron peaks for spacecraft charge. The energy flux is adjusted for the estimated -5.6 volt spacecraft charge.

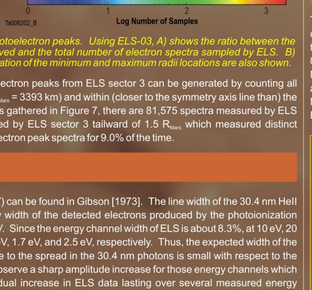

Figure 6. Adjusted tail electron spectra showing degraded photoelectron peaks for spacecraft charge. The energy flux is adjusted for the estimated -5.6 volt spacecraft charge.

3. Electron Outflow

Estimation of the electron outflow from Mars is determined by examining the occurrence frequency of electrons flowing out of the tail. The estimation process uses the fact that the signal is narrow with respect to the energy width. The outflow frequency is normalized by the example spectrum, taking into account the average angular width of detection. A final estimate is achieved by estimating the area through which these electrons flow.

3.1. Tail Photoelectron Peak Frequency

The MEx ELS was used to gather occurrence frequencies of the observation of peaks in the photoelectrons primarily caused by the dayside atmospheric ionization of carbon dioxide and atomic oxygen [Frahm *et al.*, 2006b]. These statistics were generated for all those measurements which showed discrete photoelectron peaks (similar to those shown in Figures 3 and 5) between 5 January 2004 and 13 November 2004. Extending the sample collection period to 25 January 2005, the updated frequency of occurrence statistics is shown in Figure 7. These data are presented in cylindrical MSO coordinates with the Sun at the right, tracing the orbit of the MEx spacecraft in a format similar to Figure 1. For these data, all orbital locations of MEx when ELS measured spectra are shown in Figure 7b (color coded by the number of samples of the electron spectrum made by ELS), while in Figure 7a, only those spectra showing distinct photoelectron spectra in ELS sector 3 are included (color coded by the fraction of spectra which showed distinct photoelectron peaks).

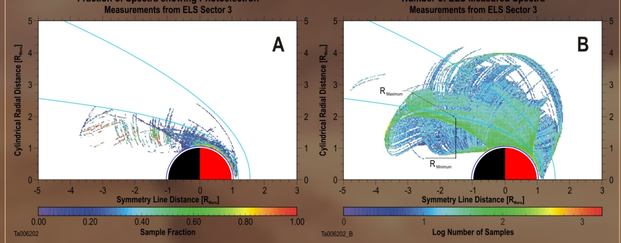

Figure 7. Statistics on the occurrence of observations of distinct photoelectron peaks. Using ELS-03, A) shows the ratio between the number of samples where distinct photoelectron peaks were observed and the total number of electron spectra sampled by ELS. B) shows the total number of electron spectra sampled by ELS. The location of the minimum and maximum radii locations are also shown.

An estimate of the total fraction of spectra showing distinct photoelectron peaks from ELS sector 3 can be generated by counting all spectra showing distinct photoelectron peaks tailward of 1.5 R_{Mars} (R_{Mars} = 3393 km) and within (closer to the symmetry axis line than) the averaged MPB determined by Vignes *et al.* [2000]. For the statistics gathered in Figure 7, there are 81,575 spectra measured by ELS sector 3 tailward of 1.5 R_{Mars} and there are 7331 spectra measured by ELS sector 3 tailward of 1.5 R_{Mars} which measured distinct photoelectron peaks. Thus, in 2004, ELS measured distinct photoelectron peak spectra for 9.0% of the time.

3.2. Line Width

The solar spectrum at and in the neighborhood of 30.4 nm (40.79 eV) can be found in Gibson [1973]. The line width of the 30.4 nm HeII line is about 0.1 nm, or ± 0.07 eV. Translating this into an energy width of the detected electrons produced by the photoionization process gives an uncertainty in the electron energy of about ± 0.07 eV. Since the energy channel width of ELS is about 8.3%, at 10 eV, 20 eV, and 30 eV the widths of the ELS energy channels are about 0.8 eV, 1.7 eV, and 2.5 eV, respectively. Thus, the expected width of the photoelectrons generated from the photoionization process just due to the spread in the 30.4 nm photons is small with respect to the energy channel width of the ELS instrument. We should expect to observe a sharp amplitude increase for those energy channels which contain the photoionized electrons (distinct) as opposed to a gradual increase in ELS data lasting over several measured energy channels.

3.3. Number of Electrons Emitted From Photoionization

Each datum is labeled with a reference number, 0 to 8, as shown in Figure 8. In order to estimate the number of photoelectrons generated by the HeII 30.4 nm line, we draw a continuous line between points 1 and 7 in log space, determine the differential number flux (DNF) values along this line for the intervening points (DEF(E') = E'·DNF(E')), and then find the number intensity beneath the line. This we will take as the background spectrum and the area is 9.04×10^7 electrons/(cm^2 s sr). The contribution due to both the background and the contribution of the HeII 30.4 nm line is 1.48×10^7 electrons/(cm^2 s sr). Thus, the portion of the number intensity which is due to the presence of the HeII 30.4 nm line is just the difference, or 5.74×10^6 electrons/(cm^2 s sr). The uncertainty in the number of electrons generated by the HeII 30.4 nm line is estimated by determining the maximum and minimum area differences. The minimum (maximum) difference is determined using the same scheme as described above except the background line is figured by drawing the line between point 1's maximum (minimum) uncertainty value and point 7's maximum (minimum) uncertainty. The background plus HeII 30.4 nm line contribution is determined by using the same values for points 1 and 7, while on points 2-6, using the minimum (maximum) uncertainty value. Thus, the minimum (maximum) difference is 4.48×10^6 (7.00×10^6) electrons/(cm^2 s sr). Combining all of our estimates, the number of electrons generated by the presence of the HeII 30.4 nm line due to ionization of carbon dioxide and atomic oxygen is $5.74 \times 10^6 \pm 1.26 \times 10^6$ electrons/(cm^2 s sr).

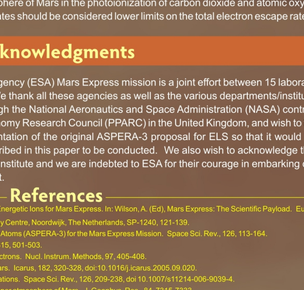

Figure 8. Integration details for the distinct photoelectron peaks. Integrations are carried out after computing the differential number flux where points involved in integration are labeled and called out in the text. Shaded area represents additional electrons from photoionization.

3.4. Angular Measurement Range

At 1.5 R_{Mars}, the number of ELS sectors which show the photoelectron peak signature is typically between 1 and 3; however, at times the signal of the peaks is observed in more ELS sectors. So, being conservative, the angular area in a cone which includes two ELS sectors, is used (radii of the cone of 22.5º), corresponding to the angular width of one ELS sector. This angular area for two filled sectors is 0.478 sr. Here we will take the uncertainty in angle of half an angular channel width, or 11.25º, giving an angular area of coverage of 0.478 ± 0.235 sr. This gives a number flux of $2.74 \times 10^7 \pm 1.47 \times 10^7$ electrons/(cm^2 s) which are escaping Mars. Since we know that in 2004, escape occurred 9.0% of the time, then an estimate of the average loss of electrons is $2.47 \times 10^7 \pm 1.32 \times 10^7$ electrons/(cm^2 s).

3.5. Tail Area Outflow

The surface area through which electrons escape Mars covers only the region measured by MEx. In three-dimensional space, there are locations which were not measured [see Frahm *et al.*, 1996b]. For this reason, we collapse the ELS measurements into the two-dimensional plane and estimate the outflow as if the outflow were symmetric. The count statistics are considered to reflect both a spatial and temporal frequency of occurrence rates. Estimating the MSO radius which contained measurements, the location of MEx in the tail was projected on to the X_{MSO} = -1.5 R_{Mars} surface, which was determined to be $R_{Maximum}$ = 2850 km (refer to Figure 7b). Due to the density of measurements, samples were found to occur to the radius of the average MPB position at X_{MSO} = -1.5 R_{Mars}, a radial distance of $R_{maximum}$ = 6700 km. This gives an estimated annular area of 1.16×10^{19} cm^2 which allows an estimation of the escape rate of the photoionized electrons at $2.85 \times 10^{27} \pm 1.53 \times 10^{27}$ electrons/s. Now 2004 contained about 3.17×10^7 s, which gives about $8.99 \times 10^{30} \pm 4.83 \times 10^{30}$ electrons that escape Mars. This represents a loss of about 15 ± 8 Mmole of electrons lost from the atmosphere of Mars just in the photoionization of carbon dioxide and atomic oxygen from the solar HeII 30.4 nm line.

4. Conclusion

A MEx orbit showing photoelectron peaks caused by the He 30.4 nm photoionization of carbon dioxide and atomic oxygen is shown as representative of cases where these photoelectron peaks appear in the ELS data. The particular pass chosen shows distinct photoelectron peaks in the ionosphere, degraded photoelectron peaks in the tail close to the inner magnetosheath boundary, and distinct photoelectron peaks at lower altitudes in the Martian tail. Consideration of energy offsets from theoretical values of distinct peaks in the dayside ionosphere as well as the tail can provide an estimate of the charge on the spacecraft. For peaks in the ionosphere of this orbit, the spacecraft charge level changes with altitude, but appears fairly steady in the Martian tail where photoelectron peaks are observed. Estimation of the spacecraft charge allows correction of the electron spectrum.

The corrected electron spectrum from the Martian tail can be used as a representative spectrum, the number of electrons escaping the planet from the ionization process is computed to be $2.74 \times 10^7 \pm 1.47 \times 10^7$ electrons/(cm^2 s). Statistics gathered on the frequency of spectra show that these photoelectron peaks occur about 9% of the time during 2004. Thus the outflow of electrons is estimated to be $2.47 \times 10^7 \pm 1.32 \times 10^7$ electrons/(cm^2 s) during 2004. An estimate of the outflow area, 1.16×10^{19} cm^2, allows estimation of the electron escape rate of $2.85 \times 10^{27} \pm 1.53 \times 10^{27}$ electrons/s caused by the ionization of carbon dioxide and atomic oxygen by the HeII 30.4 nm line during 2004. This can be expressed as the total number of electrons that escape in 2004 as about $8.99 \times 10^{30} \pm 4.83 \times 10^{30}$ electrons or about 15 ± 8 Mmole of electrons lost from the atmosphere of Mars in the photoionization of carbon dioxide and atomic oxygen caused by the solar HeII 30.4 nm line. These derived escape rates should be considered lower limits on the total electron escape rate from Mars

Acknowledgments

The ASPERA-3 experiment on the European Space Agency (ESA) Mars Express mission is a joint effort between 15 laboratories in 10 countries, all sponsored by their national agencies. We thank all these agencies as well as the various departments/institutes hosting these efforts. We wish to acknowledge support through the National Aeronautics and Space Administration (NASA) contract NASW-00003 in the United States, Particle Physics and Astronomy Research Council (PPARC) in the United Kingdom, and wish to thank those NASA officials who had the foresight to allow augmentation of the original ASPERA-3 proposal for ELS so that it would provide the additional capabilities which allowed the science described in this paper to be conducted. We also wish to acknowledge the Swedish National Space Board for their support of the main PI-institute and we are indebted to ESA for their courage in embarking on the Mars Express program, the first ESA mission to the red planet.

References

Barabash, S., *et al.*, 2004. ASPERA-3: Analyser of Space Plasmas and Energetic Ions for Mars Express. In: Wilson, A. (Ed), Mars Express: The Scientific Payload. European Space Agency Publications Division, European Space Research & Technology Centre, Noordwijk, The Netherlands, SP-1240, 121-139.

Barabash, S., *et al.*, 2006. The Analyzer of Space Plasmas and Energetic Atoms (ASPERA-3) for the Mars Express Mission. Space Sci. Rev., 126, 113-164.

Barabash, S., *et al.*, 2007. Martian atmospheric erosion rates. Science, 315, 501-503.

Bordoni, F. 1971. Channel electron multiplier efficiency fo 10-1000 eV electrons. Nucl. Instrum. Methods, 97, 405-408.

Carlsson, E., *et al.*, 2006. Mass composition of the escaping plasma at Mars. Icarus, 182, 320-328, doi:10.1016/j.icarus.2005.09.020.

Dubinin, E., *et al.*, 2006. Plasma morphology at Mars. ASPERA-3 observations. Space Sci. Rev., 126, 209-238, doi 10.1007/s11214-006-9039-4.

Fox, J. L., Dalgarno, A., 1979. Ionization, luminosity, and heating of the upper atmosphere of Mars. J. Geophys. Res., 84, 7315-7333.

Frahm, R. A., *et al.*, 2006a. Carbon dioxide photoelectron energy peaks at Mars. Icarus, 182, 371-382.

Frahm, R. A., *et al.*, 2006b. Locations of atmospheric photoelectron energy peaks within the Mars environment. Space Sci. Rev., 126, 389-402, DOI 10.1007/s11214-006-9119-5.

Gibson, E. G., 1973. The Quiet Sun, NASA SP-303, National Aeronautics and Space Administration, Washington, D.C.

Liemohn, M. W., *et al.*, 2006a. Numerical interpretation of high-altitude photoelectron observations. Icarus, 182, 383-395.

Liemohn, M. W., *et al.*, 2006b. Mars global MHD predictions of magnetic connectivity between the dayside ionosphere and the magnetospheric flanks. Space Sci. Rev., 126, 63-76.

Lundin, R., *et al.*, 1989. First measurements of the ionospheric plasma escape from Mars. Nature, 341, 609-611.

Lundin, R., *et al.*, 1990. Plasma composition measurements of the Martian magnetosphere morphology. Geophys. Res. Lett., 17, 877-880.

Lundin, R., *et al.*, 2004. Solar wind-induced atmospheric erosion on Mars: First results from ASPERA-3 on Mars Express. Science, 305, 1933-1936.

Mantas, G. P., Hanson. W. B., 1979. Photoelectron fluxes in the Martian ionosphere. J. Geophys. Res., 84, 369-385.

Padial, N., *et al.*, 1981. Photoexcitation and ionization in carbon dioxide: Theoretical studies in the separated-channel static-exchange approximation. Phys. Rev. A, 23, 218-235.

Verigin, M. I., *et al.*, 1991. Ions of planetary origin in the Martian magnetosphere (Phobos 2/TAUS experiment). Planet. Space Sci., 29, 131-137.

Vignes, D., *et al.*, 2000. The solar wind interaction with Mars: Locations and shapes of the bow shock and the magnetic pile-up boundary from observations of the MGS/ER experiment on board Mars Global Surveyor. Geophys. Res. Lett., 27, 49-52.

Pa0520